

Modifying Native Nanocellulose Aerogels with Carbon Nanotubes for Mechanoresponsive Conductivity and Pressure Sensing

Miao Wang, Ilya V. Anoshkin, Albert G. Nasibulin, Juuso T. Korhonen, Jani Seitsonen, Jaakko Pere, Esko I. Kauppinen, Robin H.A. Ras,* and Olli Ikkala*

Highly porous aerogels, skeleton-like or sponge-like materials have aroused considerable recent interest towards various functional properties, such as lightweight construction, thermal and acoustic insulation, membranes, separation, chemical analysis, catalyst support, sensing, energy technologies, and energy absorption.^[1–32] The first aerogels were demonstrated already early^[33] and an extensive literature exists based on silica gels, sol-gel materials, cross-linked polymers, regenerated cellulose, and pyrolyzed carbon-based materials, as reviewed in refs.^[34,35] Aerogels are usually prepared from solvent-swollen gel networks by removing the solvent, taken that the network collapse can be suppressed by freeze-drying or supercritical drying. The air- or gas-filled skeleton structure can allow very low densities down to ca. 10 mg/cm³ or less, high porosities in excess of 95%, and even high surface areas. As the classic routes tend to be brittle, which can reduce application potential, there has been extensive search for ductile and flexible aerogels using nanofibers. In particular, reduced brittleness and even flexibility have been shown using native cellulose nanofiber aerogels, based on nanofibrillated cellulose (NFC), also called microfibrillated cellulose (MFC) or using bacterial cellulose.^[6,12] NFC is particularly attractive due to its enhanced mechanical properties with a modulus in the range 140 GPa^[36] and as cellulose is sustainable and the most abundant polymer on Earth, as available from plant cell walls.^[37] Importantly, to preserve the native crystalline form, specific processes have been developed to cleave the 3–20 nm diameter nanofibers from plant cell walls without dissolution in practical ways.^[38–40] Also for carbon nanotubes (CNTs) several approaches have recently been described to prepare aerogels.^[3–5,7,9,13–15,17,21–23,27–32] Therein, in a typical solvent-based process, CNTs are first chemically or physically functionalized or mixed with binder polymers to increase the nanotube-nanotube interactions which, in turn, promote

gelation and finally lead to aerogel formation upon freeze-drying or supercritical drying. But interestingly, gas phase synthesis can lead to CNT elastic sponges even without binders and cross-links obviously due to entanglements.^[14,15] Such sponges allow also pressure sensing in compression as the resistance depends on the strain level, reflecting the importance of the electrical contacts between the nanotubes, i.e., electrical percolation for the overall electrical behavior. However, even if CNT aerogels show exciting properties, their production in bulk quantities poses challenges.

Here we combine the best aspects of NFC and CNT aerogels in their hybrids in a synergistic manner, both forming separately aerogels, as described above. In more detail, we foresee that the mechanically excellent NFC nanofibers, as available from widely abundant sustainable plant-based sources and facile processes could be templates for functionalization by small weight fractions of CNT, thus combining the bulk availability of NFC and advanced electrical properties of CNT. Such hybrid nanocomposite aerogels have not yet been presented.

NFC nanofibers were prepared from an aqueous native birch pulp by first grinding and then passing 16 times through a homogenizer, essentially as reported elsewhere.^[6] After such a process, the entangled nanofibers have diameter of ca. 9 nm and it forms an aqueous suspension of a concentration of 1.7 wt%. Importantly it forms a hydrogel, as described before,^[38] see schematics in **Figure 1a**. Regarding larger scale applications, few-walled carbon nanotubes (FWCNT) were selected instead of single-walled nanotubes, having intact inner layers after chemical modifications. They were produced by catalytic pyrolysis of CH₄ in the presence of H₂ at 960 °C on the (Co-Mo)/MgO catalyst (see Supporting Information), as described previously.^[41] They have diameter of 3–7 nm, see **Figure 1e**. In order to promote dispersibility in water, FWCNTs were surface functionalized by oxygen containing groups (mostly -COOH, >C=O, and -OH), see Supporting Information.^[42] For simplicity, the functionalized nanotubes are subsequently still denoted as FWCNTs. An aqueous dispersion of FWCNT of the concentration of 0.4 wt% is added into the NFC hydrogel, followed by mixing with a high-speed mixer and ultrasonic bath (**Figure 1b**). The emphasis was in the composite hydrogel compositions where the NFC forms the majority phase, i.e., NFC/FWCNT 100/0, 95/5, 90/10, 85/15, 80/20, 75/25 w/w. The pure FWCNT hydrogel was obtained by increasing the concentration to 2.0 wt%, followed by mixing with a high-speed mixer and ultrasonic bath. This leads to macroscopically essentially homogeneous suspensions by visual inspection.

M. Wang, Dr. I. V. Anoshkin, Dr. A. G. Nasibulin,
J. T. Korhonen, Dr. J. Seitsonen, Prof. E. I. Kauppinen,
Dr. R. H. A. Ras, Prof. O. Ikkala
Department of Applied Physics
Aalto University School of Science (formerly Helsinki
University of Technology)
FIN-00076 Aalto, Espoo, Finland
E-mail: robin.ras@aalto.fi; olli.ikkala@aalto.fi
Dr. J. Pere
VTT Technical Research Centre of Finland
Biotechnology, FIN-02044 VTT, Finland



DOI: 10.1002/adma.201300256

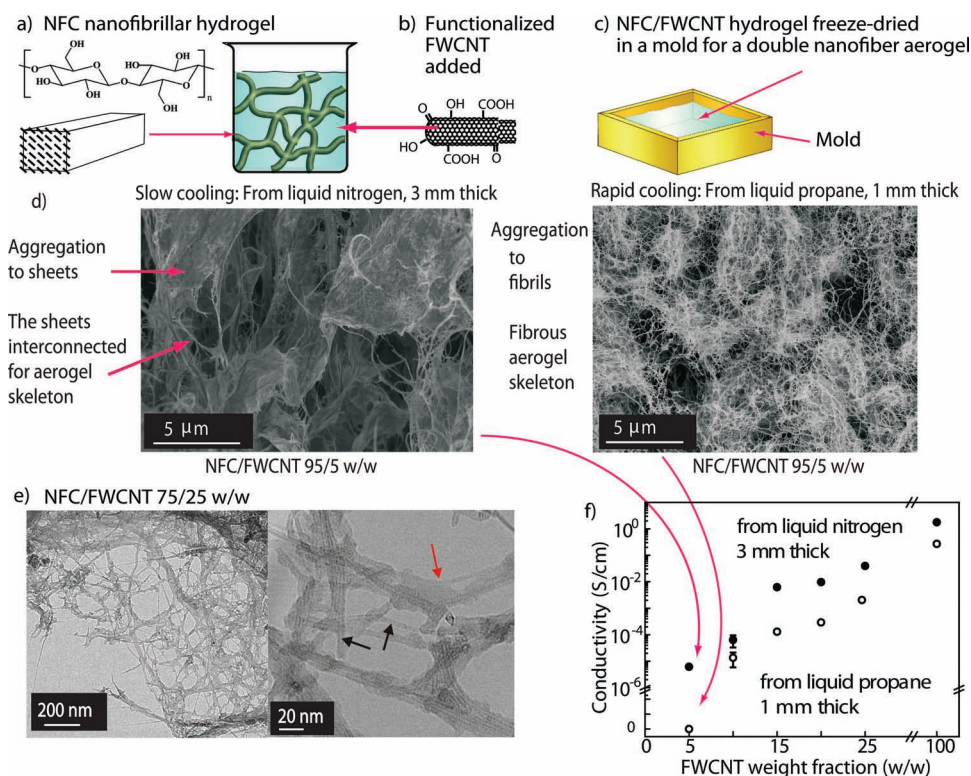


Figure 1. a) Nanofibrillated cellulose (NFC) forms strong physical gels in aqueous medium due to the long and entangled hydrogen bonded native cellulose nanofibers of diameters in the nanometer range. b) Few-walled carbon nanotubes (FWCNTs) are modified to allow dispersion in the aqueous medium, mixed in the NFC hydrogel and homogenized by ultrasound treatment. c) The hybrid NFC/FWCNT hydrogel is inserted in a mold, and cooled by plunging into liquid propane or liquid nitrogen and freeze-dried to allow aerogels. d) Freeze-drying from liquid nitrogen leads to slow cooling and to sheet-like morphology due to aggregation of NFC and FWCNT, whereas freeze-drying from liquid propane leads to quicker cooling and to fibrillar morphology. e) Cryo-TEM images of NFC/FWCNT 75/25 w/w aerogel; at high magnification the FWCNT (black arrow) can be distinguished from NFC (red arrow). It is clear that NFC and FWCNT are in close contact. f) Conductivity of NFC/FWCNT aerogels.

The aerogels were next prepared by freeze-drying. The hybrid hydrogels were positioned in a mold, which was then rapidly immersed in a cryogenic fluid for cooling and freezing followed by insertion in a vacuum chamber on a pre-cooled metal support plate and pumping to remove the ice by sublimation (see Figure 1c and Supporting Information). The procedures are similar as described for pure NFC aerogels previously.^[6] In the first protocol, liquid nitrogen (boiling point $-196\text{ }^{\circ}\text{C}$) was used for cooling and relatively thick (3 mm) samples of lateral dimensions $14\text{ mm} \times 5\text{ mm}$ were used. After freeze-drying, the morphologies were inspected by scanning electron microscopy (SEM). Figure 1d shows the SEM micrograph for the NFC/FWCNT 95/5 w/w aerogel as a characteristic example. Sheet-like structures of micrometer lateral dimensions are observed, as connected by nanofiber bundles of up to ca. 100 nm diameter. The sheet-like aggregation can be qualitatively explained, as upon immersing the room-temperature aqueous gel sample in liquid nitrogen leads to a thin thermally insulating N_2 -gas layer on the sample surface (the so-called Leidenfrost effect), thus slowing down the heat transfer between the sample and the cryogenic fluid.^[18] This, in combination with the relatively large selected sample thickness causes slow cooling. Therefore, the ice crystals have time to grow during the cooling and they become large. This promotes the aggregation of nanofibrils into sheets, as known for NFC.^[6] But also FWCNT has a tendency to

form large sheets due to aggregation upon immersing in liquid nitrogen (see Supporting Information Figure S2a, c). The question arises whether NFCs and FWCNTs aggregate into separate nanosheets or form hybrid nanosheets. Due to their roughly similar diameter, it is difficult to recognize individual NFC and FWCNT nanofibers in the sheets by SEM observation. Indirect observations point towards composite sheets: the pure FWCNT aerogels as freeze dried in a similar fashion, show sheets with characteristically sharp edges (Figure S2c), not observed in the hybrid aerogels (see e.g. composite Figure 1d), thus suggesting co-aggregation. This would not be surprising, as benzene rings and cellulose have direct affinity^[43] and the present surface functionalization of FWCNT also promotes hydrogen bonding to NFC. The sheet-like morphology of NFC and FWCNT would have an important role in the electrical properties, to be discussed later. In another freeze-drying protocol, liquid propane (boiling point $-42\text{ }^{\circ}\text{C}$) cooled to liquid nitrogen temperature is used for cooling, leading to no thermally insulating boiling gas layer.^[18] Selecting sufficiently thin samples (1 mm) a relatively quick cooling results. This leads to drastically different morphology, as no sheet-like fibrillar aggregates are formed, as shown for 1 mm thick NFC/FWCNT 95/5 w/w aerogel (Figure 1d). The ice crystals are now smaller and the nanofibrillar network structure is mostly preserved upon freezing and sublimation of ice. Also for pure FWCNT aerogels, the

sheet forming tendency is smaller for the liquid propane freeze-drying than in the case of liquid nitrogen freeze-drying (Supporting Information Figure S2b,d).

Transmission electron microscopy (TEM) was used in an effort to resolve the individual NFC nanofibers and FWCNT nanotubes. In this respect, the composition NFC/FWCNT 75/25 w/w turned most feasible, as it contained relatively large fraction of FWCNT, see Figure 1e. Liquid propane freeze drying was used to preserve fibrous structure. Figure 1e shows individual FWCNTs of diameter of ca. 3 nm and NFCs of lateral dimensions of ca. 9 nm. The figure also indicates that there exists an intimate contact between the FWCNT and NFC, due to their expected interaction, as described above.

The electrical conductivities of NFC/FWCNT aerogels are shown in Figure 1f for the two freeze-drying methods. Pure NFC aerogels are not conductive whereas the pure FWCNT aerogel has an electrical conductivity of $1.8 \text{ S} \cdot \text{cm}^{-1}$ upon liquid nitrogen freeze-drying and an order of magnitude less for the liquid propane freeze-drying. In the hybrid aerogels the electrical conductivity increases upon increasing the FWCNT weight fraction, and liquid nitrogen freeze-dried NFC/FWCNT 80/20 w/w aerogel shows a relatively high electrical conductivity of $1 \times 10^{-2} \text{ S} \cdot \text{cm}^{-1}$. The sheet-like architectures, as observed for the liquid nitrogen freeze-dried samples of thickness 3 mm, show higher conductivities in all cases than the corresponding compositions following the liquid propane freeze-drying of 1 mm thick aerogels having the fibrillar structure. This observation was particularly clear for the composition NFC/FWCNT 95/5 w/w, which did not conduct based on liquid propane freeze-drying. We tentatively assign the higher conductivity in case of the sheet architecture for a subtle hierarchical percolation: At the smaller length scale, the FWCNTs percolate within the essentially 2-dimensional aggregate sheets within the NFC matrix, and in the larger scale these essentially 2-dimensional conducting sheets percolate in the 3-dimension aerogel overall volume, also connected by fibrillar NFC and FWCNT. Therefore, we concentrate in the following solely on aerogels involving sheet-like architecture as achieved by the slow cooling in freeze-drying by the liquid nitrogen freeze-drying and thick samples.

The stress-strain curves under compression are shown in Figure 2 for the liquid nitrogen freeze-dried aerogels involving sheet-like architecture up to FWCNT concentration of 20 w/w having approximately a constant density $\approx 0.02 \text{ g cm}^{-3}$ (see Table 1). The pure NFC aerogel has an essentially linear stress-strain curve at low strains without yield point and the maximum compression strain 70% is observed. This indicates a ductile behavior of pure NFC aerogels with reduced brittleness, as expected from previous works for NFC.^[6] Upon adding FWCNTs the shape of the stress-strain curve remains qualitatively similar, but the stress levels curiously become reduced and the maximum strain increases to 95% for the FWCNTs content approaching 20 w/w. In other words, replacing part of NFCs by FWCNTs in the compositions leads to plasticization, which is at first slightly surprising. But this might be explained by the smaller number of interaction sites in the functionalized FWCNT in comparison to the extensive amount of hydroxyl groups of NFCs, i.e., a FWCNT binds weaker with its local surrounding. The inset shows the stress-strain curve

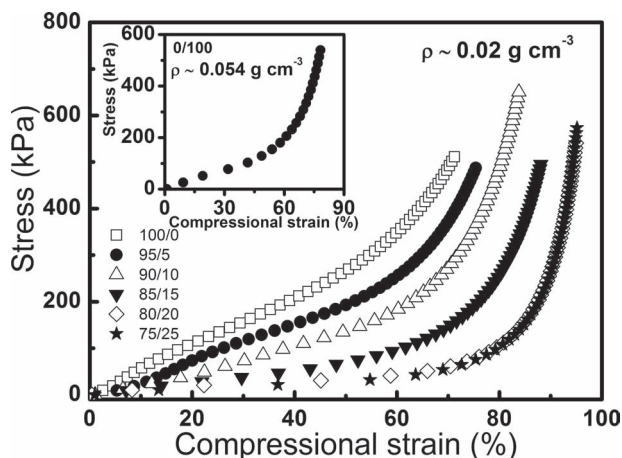


Figure 2. Compression stress-strain curves of hybrid NFC/FWCNT aerogels (The density is in the range 0.02 g cm^{-3}). For reference, the inset depicts the pure FWCNT aerogel (density $\rho \approx 0.054 \text{ g cm}^{-3}$), which did not allow low-density aerogels without collapse.

for pure FWCNT. But importantly, without added NFC, the pure FWCNT underwent some shrinkage after ice sublimation, which leads to higher density $\approx 0.054 \text{ g cm}^{-3}$. This effect can be explained by the strong π - π interaction which leads to the tendency to form FWCNT bundles. Therefore, NFC templating allowed reaching lower densities ca. $0.01 - 0.02 \text{ g cm}^{-3}$ in the composite aerogels.

Finally, the electrical properties upon compression were investigated using aerogels with sheet-like structure by liquid nitrogen freeze-drying. The aerogel was clamped between two conducting electrodes, and pressure was exerted by dry N_2 -gas. Figure 3a shows the relative resistance change vs imposed pressure for the aerogel NFC/FWCNT 75/25 w/w having the density $\approx 0.01 \text{ g cm}^{-3}$. A change of pressure of 0.1 bar induces a 10% relative change in the resistance. The stability is demonstrated by cycled 0.5 bar pressure. For comparison, for NFC/FWCNT 80/20 w/w having almost double density $\approx 0.018 \text{ g cm}^{-3}$ but smaller weight fraction of FWCNT, an almost similar compression stress strain curve was observed. Regarding

Table 1. Mechanical properties of the NFC/FWCNT aerogels with different FWCNT weight fraction. Data refer to mean values and corresponding standard deviations in brackets of at least five samples. Density and porosity calculations are described in Supporting Information.

FWCNT weight fraction [% w/w]	density [g cm^{-3}]	porosity [%]	maximum compression strain [%]	compression strength [kPa]	specific compression modulus [$\text{MPa g}^{-1} \text{ cm}^3$]
0	0.024	98.4	70 (2.3)	522 (29)	22 (1.2)
5	0.023	99.2	73 (2.2)	497 (38)	22 (1.7)
10	0.022	99.3	83 (1.3)	651 (59)	30 (2.7)
15	0.015	99.5	88 (1.1)	510 (47)	34 (3.2)
20	0.018	99.4	95 (0.4)	548 (86)	30 (4.3)
25	0.010	99.7	94 (1.2)	567 (76)	41 (15.4)
100	0.054	96.4	82 (2.3)	549 (81)	10 (1.5)

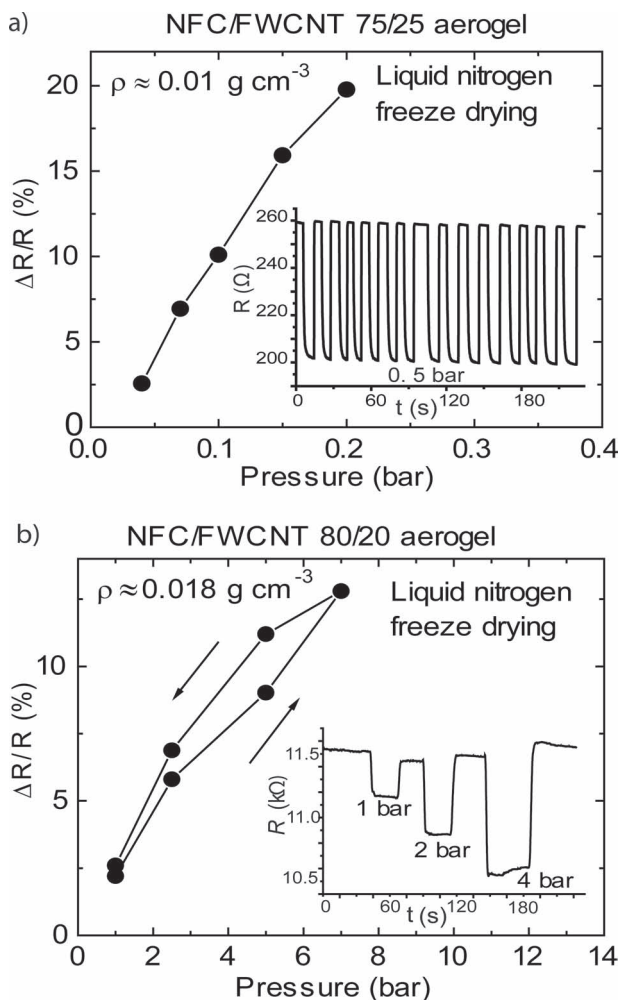


Figure 3. The absolute resistance changes of hybrid NFC/FWCNT aerogels as a function of exerted hydrostatic pressure by pressurized N_2 gas. The samples have been prepared by liquid nitrogen freeze-drying, thus leading to sheet-like morphology. a) FWCNT loading of 25 w/w allows high sensitivity of even small pressures whereas b) for lower FWCNT loading 20 w/w higher pressures are needed to allow significant absolute resistance changes and removing pressure leads to small hysteresis.

the resistance change under pressure, a qualitatively similar behavior was also here observed (Figure S4, Supporting Information), but in order to achieve 10% relative change in resistance, the imposed pressure has to be ca. 5 bar. This indicates the complex interplay within the overall percolation, as effected by the mechanical percolation by the aerogel structure and density, and the electrical percolation as controlled by the CNT concentration, and the hierarchical percolation due to the sheet formation. We finally point out that addition of NFC was essential, as without NFC, the resistance did not behave reproducibly under compression using the present FWCNTs (Figure S5, Supporting Information). Previously related mechanically elastic and electrically reversible compressional behavior has been achieved using aerogel compositions where CNT or graphene form the majority phases, including minor fraction of binders or cross-linkers or also using subtle chemical vapor deposition concepts.^[13–15,21,23] By contrast, the present hybrid

nanofiber/nanotube aerogel concept shows qualitatively similar behavior using only a minor fraction of the more precious FWCNTs by combining with the nanocellulosic fibers. Taken the abundant availability of NFC, and the robustness, the concept is attractive. Also, NFC is herein the main source for good elastic mechanical properties whereas FWCNTs are responsible for the electrical properties, thus showing synergism between the nanofibers and nanotubes within the aerogels.

In summary, incorporating both NFC and CNT within the aerogels allows to combine the attractive features of both components: the wide availability, easy processing, and sustainability of the NFC majority component and the advanced electrical properties of the CNT minority component. In this letter we have described the first such hybrid aerogels, denoted here as hybrid nanofiber/nanotube aerogels, where both components have the tendency to form aerogels separately. The aerogels have been freeze-dried from aqueous hybrid gels. The hybrid nanofiber/nanotube aerogels are ductile, with reduced brittleness, as promoted by the particular native structure of NFC, which is retained by directly cleaving it from plant cell walls without dissolution steps. The aerogel morphology can be tuned by the freeze-drying process, as slow cooling by immersion of a hydrogel sample into liquid nitrogen leads to nanofiber aggregation into sheets, whereas quick cooling in liquid propane suppresses the sheet formation and allows fibrils in thin samples. We foresee that combining nanocellulose and carbon nanotubes allows a wide variety of responsive electroactivity, pressure sensing, and functional materials, combining the best aspects of both components even towards larger scale applications.

Experimental Section

Experimental details are given in the Supporting Information.

Supporting Information

Supporting Information is available from the Wiley Online Library or from the author.

Acknowledgements

We acknowledge Academy of Finland, Finnish Funding Agency for Technology and Innovation (TEKES, projects Naseva and LIBACAM 211247), National Nanocellulose Center (Finland), UPM Corporation, and ERC for funding. This work made use of the Aalto University Nanomicroscopy Center (Aalto-NMC) premises.

Received: January 17, 2013
 Published online: March 1, 2013

- [1] C. Tan, B. M. Fung, J. K. Newman, C. Vu, *Adv. Mater.* **2001**, *13*, 644–646.
- [2] R. Fu, B. Zheng, J. Liu, M. S. Dresselhaus, G. Dresselhaus, J. H. Satcher Jr., T. F. Baumann, *Adv. Funct. Mater.* **2003**, *13*, 558–562.
- [3] D. Zhang, L. Shi, J. Fang, K. Dai, X. Li, *Mater. Chem. Phys.* **2006**, *97*, 415–419.

- [4] M. B. Bryning, D. E. Milkie, M. F. Islam, L. A. Hough, J. M. Kikkawa, A. G. Yodh, *Adv. Mater.* **2007**, *19*, 661–664.
- [5] J. M. Romo-Herrera, M. Terrones, H. Terrones, S. Dag, V. Meunier, *Nano Lett.* **2007**, *7*, 570–576.
- [6] M. Pääkkö, J. Vapaavuori, R. Silvennoinen, H. Kosonen, M. Ankerfors, T. Lindström, L. A. Berglund, O. Ikkala, *Soft Matter* **2008**, *4*, 2492–2499.
- [7] M. A. B. Meador, S. L. Vivod, L. McCorkle, D. Quade, R. M. Sullivan, L. J. Ghosn, N. Clark, L. A. Capadona, *J. Mater. Chem.* **2008**, *18*, 1843–1852.
- [8] A. J. Svagan, M. A. S. Azizi Samir, L. A. Berglund, *Adv. Mater.* **2008**, *20*, 1263–1269.
- [9] M. A. Worsley, P. J. Pauzaskie, S. O. Kucheyev, J. M. Zaug, A. V. Hamza, J. H. Satcher Jr., T. F. Baumann, *Acta Mater.* **2009**, *57*, 5131–5136.
- [10] M. D. Gawryla, O. van den Berg, C. Weder, D. A. Schiraldi, *J. Mater. Chem.* **2009**, *19*, 2118–2124.
- [11] L. Heath, W. Thielemans, *Green Chem.* **2010**, *12*, 1448–1453.
- [12] R. T. Olsson, M. A. S. Azizi Samir, G. Salazar-Alvarez, L. Belova, V. Ström, L. A. Berglund, O. Ikkala, J. Nogués, U. W. Gedde, *Nature Nanotech.* **2010**, *5*, 584–588.
- [13] J. Zou, J. Liu, A. S. Karakoti, A. Kumar, D. Joung, Q. Li, S. I. Khondaker, S. Seal, L. Zhai, *ACS Nano* **2010**, *4*, 7293–7302.
- [14] X. Gui, A. Cao, J. Wei, H. Li, Y. Jia, Z. Li, L. Fan, K. Wang, H. Zhu, D. Wu, *ACS Nano* **2010**, *4*, 2320–2326.
- [15] X. Gui, J. Wei, K. Wang, A. Cao, H. Zhu, Y. Jia, Q. Shu, D. Wu, *Adv. Mater.* **2010**, *22*, 617–621.
- [16] F. Liebner, E. Haimer, M. Wendland, M.-A. Neouze, K. Schlufner, P. Miethe, T. Heinze, A. Potthast, T. Rosenau, *Macromol. Biosci.* **2010**, *10*, 349–352.
- [17] X. Zhang, J. Liu, B. Xu, Y. Su, Y. Luo, *Carbon* **2011**, *49*, 1884–1893.
- [18] J. T. Korhonen, P. Hiekkataipale, J. Malm, M. Karppinen, O. Ikkala, R. H. A. Ras, *ACS Nano* **2011**, *5*, 1967–1974.
- [19] T. A. Schaedler, A. J. Jacobsen, A. Torrents, A. E. Sorensen, J. Lian, J. R. Greer, L. Valdevit, W. B. Carter, *Science* **2011**, *334*, 962–965.
- [20] H. Jin, M. Pääkkö, A. Laiho, H. Pynnönen, J. Paltakari, A. Marmur, O. Ikkala, R. H. A. Ras, *Langmuir* **2011**, *27*, 1930–1934.
- [21] K. H. Kim, M. Vural, M. F. Islam, *Adv. Mater.* **2011**, *23*, 2865–2869.
- [22] K. H. Kim, Y. Oh, M. F. Islam, *Nature Nanotech.* **2012**, *7*, 562–566.
- [23] Z. Xu, Y. Zhang, P. Li, C. Gao, *ACS Nano* **2012**, *6*, 7103–7113.
- [24] J. Cai, S. Liu, J. Feng, S. Kimura, M. Wada, S. Kuga, L. Zhang, *Angew. Chem. Int. Ed.* **2012**, *51*, 2076–2079.
- [25] D. Wu, F. Zhang, H. Liang, X. Feng, *Chem. Soc. Rev.* **2012**, *41*, 6160–6177.
- [26] N. Gaponik, A.-K. Herrmann, A. Eychmüller, *J. Phys. Chem. Lett.* **2012**, *3*, 8–17.
- [27] Y. Fang, F. Jiang, H. Liu, X. Wu, Y. Lu, *RSC Adv.* **2012**, *2*, 6562–6569.
- [28] S. N. Schiffres, K. H. Kim, L. Hu, A. J. H. McGaughey, M. F. Islam, J. A. Malen, *Adv. Funct. Mater.* **2012**, *22*, 5251–5258.
- [29] S. J. Shin, S. O. Kucheyev, M. A. Worsley, A. V. Hamza, *Carbon* **2012**, *50*, 5340–5342.
- [30] Z. Sui, Q. Meng, X. Zhang, R. Ma, B. Cao, *J. Mater. Chem.* **2012**, *22*, 8767–8771.
- [31] J. Zhang, Y. Cao, J. Feng, P. Wu, *J. Phys. Chem. C* **2012**, *116*, 8063–8068.
- [32] W. Zhang, Y. Zhang, C. Lu, Y. Deng, *J. Mater. Chem.* **2012**, *22*, 11642–11650.
- [33] S. S. Kistler, *Nature* **1931**, *127*, 741.
- [34] N. Hüsing, U. Schubert, *Angew. Chem. Int. Ed.* **1998**, *37*, 22–45.
- [35] A. C. Pierre, G. M. Pajonk, *Chem. Rev.* **2002**, *102*, 4243–4265.
- [36] S. Iwamoto, W. Kai, A. Isogai, T. Iwata, *Biomacromolecules* **2009**, *10*, 2571–2576.
- [37] D. Klemm, F. Kramer, S. Moritz, T. Lindström, M. Ankerfors, D. Gray, A. Dorris, *Angew. Chem. Int. Ed.* **2011**, *50*, 5438–5466.
- [38] M. Pääkkö, M. Ankerfors, H. Kosonen, A. Nykänen, S. Ahola, M. Österberg, J. Ruokolainen, J. Laine, P. T. Larsson, O. Ikkala, T. Lindström, *Biomacromolecules* **2007**, *8*, 1934–1941.
- [39] M. Henriksson, G. Henriksson, L. A. Berglund, T. Lindström, *Eur. Polym. J.* **2007**, *43*, 3434–3441.
- [40] T. Saito, S. Kimura, Y. Nishiyama, A. Isogai, *Biomacromolecules* **2007**, *8*, 2485–2491.
- [41] E. G. Rakov, I. V. Anoshkin, N. C. Khung, P. V. Saraev, A. V. Malykh, N. M. Tyong, A. S. Shinshin, M. P. Gladkova, A. L. Dubas, S. I. Pozin, *Theor. Found. Chem. Eng.* **2008**, *42*, 595–598.
- [42] N. T. Hung, I. V. Anoshkin, A. P. Dementjev, D. V. Katorov, E. G. Rakov, *Inorg. Mater.* **2008**, *44*, 219–223.
- [43] D. S. D. da Silva Perez, R. Ruggiero, L. C. Morais, A. E. H. Machado, K. Mazeau, *Langmuir* **2004**, *20*, 3151–3158.